Inorg. Chem. **2005**, *44*, 5911–5920

Ligand Substituent Effect Observed for Ytterbocene 4′-Cyano-2,2′:6′,2′′-terpyridine

Jacqueline M. Veauthier,[†] Eric J. Schelter,[†] Christopher J. Kuehl,[†] Aurora E. Clark,[‡] Brian L. Scott,[†] David E. Morris,[†] Richard L. Martin,[‡] J. D. Thompson,[§] Jaqueline L. Kiplinger,[†] and Kevin D. John*[,†]

Chemistry, Theoretical, and Materials Science and Technology Divisions, Los Alamos National Laboratory, Los Alamos, New Mexico 87545

Received January 28, 2005

A new N-heterocyclic complex of ytterbocene ($Cp^*_2Yb^{II}$, $Cp^* = C_5Me_5$) has been prepared by the addition of 4′-cyano-2,2′:6′,2′′-terpyridine (tpyCN) to $Cp^*_2Yb^{II}(OEt_2)$ in toluene to give a dark blue species designated as Cp^*_2Yb(tpyCN). The effect of the electron-withdrawing group (–C≡N) on the redox potentials of the charge-transfer form of this complex [in which an electron is transferred from the f^{14} metal center to the lowest unoccupied (π^*) molecular orbital of the tpyCN ligand to give a $4f^{13}$–π^{*1} electronic configuration] has been quantified by cyclic voltammetry. The tpyCN ligand stabilizes this configuration by 60 mV more than that in the unsubstituted tpy ligand complex and by 110 mV more than that in the unsubstituted bpy ligand complex. Magnetic susceptibility measurements corroborate the enhanced stabilization of the $4f^{13}$–π^{*1} configuration by the substituted terpyridyl ligand complex. Furthermore, the temperature dependence of the magnetic data is most consistent with a thermally induced valence tautomeric equilibrium between this paramagnetic $4f^{13}$–π^{*1} form that dominates near room temperature and the diamagnetic $4f^{14}$–π^{*0} form that dominates at low temperature. Differing coordination modes for the tpyCN ligand to the ytterbocene center have also been confirmed by isolation and X-ray crystallographic characterization of complexes binding through either the cyano nitrogen of tpyCN or the three terpyridyl nitrogen atoms of tpyCN.

Introduction

A paramagnetic electronic configuration has been reported recently for various N-heterocyclic base adducts of ytterbocene ($Cp^*_2Yb^{II}$, $Cp^* = C_5Me_5$).[1−4] The electronic structures in these complexes appear to derive from a spontaneous electron transfer from the formally $4f^{14}$ Yb^{II} metal center to the lowest unoccupied molecular orbital (LUMO) of the coordinated ligand, yielding a $4f^{13}-\pi^{*1}$ electronic configuration presumed to be the ground state at room temperature. Although the generality of the metal-to-ligand charge transfer is now established,[1−4] fundamentally interesting questions as to its origin are just beginning to be addressed.

The variable-temperature magnetic behavior of the diimine adducts of ytterbocene [e.g., $Cp^*_2Yb(L)$, L = 2,2′-bipyridine (bpy) and 1,10-phenanthroline (phen)] is one of their more unusual characteristics.[1,2] Both of the bpy and phen adducts have strongly temperature-dependent magnetic susceptibilities, but significant differences in their room-temperature magnetic moments suggest that there is a ligand-centered electronic structural basis for the difference between the two. Room-temperature magnetic moments (μ_{eff}) determined for both of the bpy and phen complexes are lower than would be predicted for noninteracting metal-centered $^2F_{7/2}$ (f^{13}) and ligand-centered $^2S_{1/2}$ (π^{*1}) spin states; i.e., the predicted μ_{eff} is 4.85 μ_B ($\chi T = 2.95$ emu K mol^{-1}), whereas the measured μ_{eff} is 2.4 μ_B ($\chi T = 0.72$ emu K mol^{-1}) for Cp^*_2Yb(bpy) and 4.0 μ_B ($\chi T = 2.0$ emu K mol^{-1}) for Cp^*_2Yb(phen).[1] The description of the magnetic behavior for these complexes is predicated on two assumptions: (1) the charge transfer of the electron from the metal ion to the imine ligand is complete, resulting in a pure $4f^{13}-\pi^{*1}$ configuration, and (2) the diminished high-temperature moments are the result of antiferromagnetic coupling between the unpaired electrons on Yb^{III} and the ligand.[1]

* To whom correspondence should be addressed. E-mail: kjohn@lanl.gov.
† Chemistry Division.
‡ Theoretical Division.
§ Materials Science and Technology Division.

(1) Schultz, M.; Boncella, J. M.; Berg, D. J.; Tilley, D.; Andersen, R. A. *Organometallics* **2002**, *21*, 460−472.
(2) Berg, D. J.; Boncella, J. M.; Andersen, R. A. *Organometallics* **2002**, *21*, 4622−4631.
(3) Da Re, R. E.; Kuehl, C. J.; Brown, M. G.; Rocha, R. C.; Bauer, E.; John, K. D.; Morris, D. E.; Shreve, A. P.; Sarrao, J. L. *Inorg. Chem.* **2003**, *42*, 5551−5559.
(4) Kuehl, C. J.; Da Re, R. E.; Scott, B. L.; Morris, D. E.; John, K. D. *Chem. Commun.* **2003**, 2336−2337.

10.1021/ic050148p CCC: $30.25
Published on Web 07/15/2005

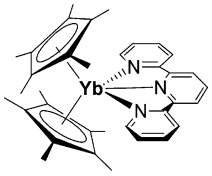

1

Figure 1. Complex **1**, [$Cp^*_2Yb(\eta^3$-tpy)].

In general, no systematic trends related to the diimine ligand structures or redox energetics have been identified to date that shed light on the origin of the charge-transfer process or the resulting spin interactions. It stands to reason that further insight into the magnetic behavior of these systems eventually may lead to a better understanding of the origin of the charge-transfer phenomenon. One possible method to explore this phenomenon experimentally is through systematic structural variations. Toward this goal, Andersen and co-workers have examined the effect of substituted cyclopentadienide ligands on the magnetic moment of the resulting complexes.[1] We recently reported the preparation of the 2,2′:6′,2″-terpyridine (tpy) adduct of ytterbocene (Figure 1).[4] This tridentate ligand was found to bind symmetrically within the ytterbocene wedge. Therefore, we became interested in tpy adducts because of the simplification provided by the symmetry of such a metal/ligand system; this geometry allows various functionalities to be directed down the main axis of the molecular assembly and/or permits introduction of various functional groups (electron-withdrawing and -donating) at the 4′ position of the coordinated terpyridine ligand.

This paper reports our study of the 4′-substituted tpy adduct of ytterbocene, 4′-cyano-2,2′:6′,2″-terpyridine (tpyCN). Our goal is to explore the effect of an electron-withdrawing group on the magnetic properties and energetics of the Cp^*_2Yb(tpy) system. The variable-temperature magnetic behavior observed for Cp^*_2Yb(tpy) and Cp^*_2Yb(tpyCN) leads us to conclude that these systems exist in a thermally induced valence tautomeric (VT) equilibrium between the diamagnetic $4f^{14}-\pi^{*0}$ and paramagnetic $4f^{13}-\pi^{*1}$ forms, with the latter charge-transfer state dominating in both systems at room temperature.

We also demonstrate that ytterbocene can bind to either type of nitrogen in tpyCN to form both monodentate and tridentate complexes in good yield. Thus, these new ytterbocene terpyridine complexes could serve as potential building blocks for multimetallic arrays or molecular materials such as those recently reported for lanthanide complexes of nitronyl nitroxides and organocyanides.[5]

Experimental Section

General Procedures. All reactions and product manipulations were carried out under an atmosphere of dry argon or helium using standard drybox or Schlenk techniques. HPLC-grade solvents were stored under argon and purified by passage through a stainless steel system consisting of either two columns of activated A2 alumina for tetrahydrofuran (THF), diethyl ether (OEt_2), and methylene chloride (CH_2Cl_2) or one column of activated A2 alumina and one column of an activated BASF R3-11 catalyst (toluene and hexanes). $Cp^*_2Yb^{II}(OEt_2)$ was prepared according to literature procedures.[6] $[Cp_2Fe^{III}]PF_6$ was purchased from Aldrich and used as received. tpyCN can be prepared according to a previously published literature procedure.[7] Potassium 4′-cyano-2,2′:6′,2″-terpyridinide, $K^+(tpyCN)^-$, was prepared by adding 1 equiv of freshly cut potassium metal to 1 equiv of tpyCN in THF and stirring overnight at room temperature. Cp^*_2Yb(tpy) (**1**) was prepared according to a previously published procedure.[4]

Infrared (IR) spectra were recorded on a Thermo-Nicolet FT-IR module instrument Magna 760 spectrometer at 4 cm^{-1} resolution as mineral oil mulls or solutions contained in an airtight sodium chloride cell (path length = 0.1 mm). GC/MS data were obtained with a Hewlett-Packard 6890 gas chromatograph configured with a DB-5 column (0.32 mm i.d. and 30 m) in series with an HP 5973 quadrupole mass detector. The column was operated at a flow rate of 0.6 mL min^{-1} and ramped between 70 and 230 °C at a rate of 20 °C min^{-1}. Elemental analyses were performed by Midwest Microlabs.

Preparation of $Cp^*_2Yb^{III}$(THF)I. $Cp^*_2Yb^{III}$(THF)I was prepared according to a modified literature procedure.[1] One equivalent of AgI (91 mg, 0.387 mmol) was added to 200 mg of $Cp^*_2Yb^{II}(OEt_2)$ (0.386 mmol) in 15 mL of THF, and the solution was stirred for 10 h at room temperature in the dark. The resulting violet solution was filtered through a glass frit and the filtrate evaporated to dryness. The solid residue was then taken up in boiling toluene, filtered hot through a glass frit, and cooled to −30 °C. The purple microcrystalline powder that formed was collected by filtration. Yield: 188 mg (0.293 mmol, 76%). The IR spectrum was consistent with that of the compound reported in the literature.[1]

Preparation of Cp^*_2Yb(tpy) (1). Cp^*_2Yb(tpy) was prepared according to a previously published procedure.[4] ^1H NMR for **1** (400.13 MHz, $C_6D_5CD_3$): (20 °C) δ 98.3 (tpy), 4.2 (tpy), −0.05 (30H, Cp*), −1.98 (tpy), −7.95 (tpy), −51.5 (tpy), other resonance not observed or obscured by solvent; (−70 °C) δ 145.0 (tpy), 106.0 (tpy), 51.0 (tpy), 27.9 (tpy), 14.8 (tpy), −1.40 (30H, Cp*), −7.30 (tpy).

Preparation of Cp^*_2Yb(tpyCN) (2). One equivalent of tpyCN (100 mg, 0.386 mmol) was added to a solution of $Cp^*_2Yb^{II}(OEt_2)$ (200 mg, 0.386 mmol) in 15 mL of toluene to give a dark blue solution that was stirred for 12 h at room temperature. The resulting suspension was filtered through a glass frit, and the blue precipitate was washed several times with cold toluene (3 × 5 mL) and *n*-hexanes (10 mL) to give **2** (247 mg, 0.351 mmol) as a blue microcrystalline powder in 91% yield. Anal. Calcd for $C_{36}H_{40}N_4Yb_1$: C, 61.61; H, 5.75; N, 7.98. Found: C, 61.78; H, 5.76; N, 7.64. IR ($\nu_{C\equiv N}$, $C_6H_5CH_3$): 2172 cm^{-1}. ^1H NMR for **2** (400.13 MHz, $C_6D_5CD_3$): (20 °C) δ 0.58 (30H, Cp*), −4.0 (tpyCN), −14.2 (tpyCN), other resonances not observed or obscured by solvent; (−70 °C) δ 42.0 (tpyCN), 19.2 (tpyCN), −3.2 (30H, Cp*), −16.2 (tpyCN), other resonances not observed or obscured by solvent.

Preparation of $[Cp^*_2Yb^{III}(tpyCN)]PF_6$ (3) and $[Cp^*_2Yb^{III}(tpyC_5Me_5)]PF_6$ (4). One equivalent of ferrocenium hexafluorophosphate (94 mg, 0.285 mmol) was added to a solution of **2** (200 mg, 0.285 mmol) in 15 mL of THF. The solution was stirred

(5) (a) Zhao, H.; Bazile, M. J.; Galán-Mascarós, J. R.; Dunbar, K. R. *Angew. Chem., Int. Ed.* **2003**, *42*, 1015−1018. (b) Raebiger, J. W.; Miller, J. S. *Inorg. Chem.* **2002**, *41*, 3308−3312. (c) Benelli, C.; Caneschi, A.; Fabretti, A. C.; Gatteschi, D.; Pardi, L. *Inorg. Chem.* **1990**, *29*, 4153−4155.

(6) Tilley, T. D.; Boncella, J. M.; Berg, D. J.; Andersen, R. A. *Inorg. Synth.* **1990**, *27*, 146−149.

(7) Potts, K. T.; Cipullo, M. J.; Ralli, P.; Theodoridis, G. *J. Org. Chem.* **1982**, *47*, 3027−3038.

overnight until it gradually became a dark red suspension. The solution was evaporated to dryness and the residue suspended in toluene. The solid material was collected on a frit and washed with toluene until the washings were colorless. The product was then extracted into CH_2Cl_2 (5 mL) and layered with *n*-pentane (15 mL) to give **3** (194 mg, 0.229 mmol) as an orange powder in 80% yield and **4** (10 mg, 0.011 mmol) as dark crystals in 4% yield as determined by GC/MS analysis (see below). IR of **3** ($\nu_{C\equiv N}$, Nujol): 2240 cm^{-1}. ^1H NMR for **3** (400.13 MHz, CD_2Cl_2, 25 °C): δ 77.0 (2H, tpy), 26.6 (2H, tpy), 25.3 (2H, tpy), 22.1 (2H, tpy), 17.2 (2H, tpy), −2.30 (30H, Cp*). We could not successfully remove all traces of **4** from samples of **3** and therefore could not obtain a clean elemental analysis of **3**. Complex **4** has been characterized by X-ray diffraction (see below).

Hydrolysis of 2−4. Approximately 5 mL of degassed H_2O was added to a solution of **2** in CH_2Cl_2, and the resulting solution was stirred for 12 h. Analysis of the GC/MS parent mass and fragmentation pattern confirmed the presence of ytterbium hydroxide, tpyCN, tpyCONH$_2$, tpyCOH, C_5Me_5H, and C_5Me_5OH in the reaction mixture. However, no tpyC_5Me_5 was observed in the GC/MS. A similar treatment was applied to the reaction mixture of **3** and **4**, revealing that 96% of the hydrolysis products associated with the polypyridyl ligands was consistent tpyCN and the remaining portion was associated with tpyC_5Me_5.

Preparation of Cp*$_2$Yb^{III}(η^1-NCtpy)I (5). One equivalent of tpyCN (80.6 mg, 0.311 mmol) was added to a solution of Cp*$_2$Yb^{III}(THF)I (200 mg, 0.311 mmol) in 15 mL of CH_2Cl_2 to give a dark purple solution that was stirred for 5 h at room temperature. The filtrate was concentrated to 5 mL and cooled to −30 °C, which led to the formation of dark purple X-ray quality crystals of **5** (see below). The product was collected on a glass frit to give 220 mg of **5** (85% yield). Anal. Calcd for $C_{36}H_{40}N_4I_1Yb_1 \cdot {}^1/_2CH_2Cl_2$: C, 50.32; H, 4.74; N, 6.43. Found: C, 50.28; H, 4.71; N, 6.46. IR ($\nu_{C\equiv N}$, Nujol): 2263 cm^{-1}. The room-temperature ^1H NMR spectrum of **5** in C_6D_6 revealed one broad resonance at δ 5.40 for the Cp* protons and several broad peaks between δ 8 and 12 for the freely rotating η^1-NCtpy ligand protons.

Preparation of [Cp*$_2$Yb^{III}(tpy)][Cp*$_2$Yb^{III}I$_2$] (6a). One equivalent of tpy (36 mg, 0.156 mmol) was added to a solution of Cp*$_2$Yb(THF)I (100 mg, 0.156 mmol) in 10 mL of toluene, which gradually changed to an orange suspension. After the orange precipitate was stirred overnight, it was collected on a glass frit and washed several times with toluene to give **6a** (93.0 mg, 0.0677 mol) as an orange powder in 87% yield. Slow diffusion of hexanes into a concentrated THF solution of **6a** gave X-ray quality crystals of **6a** (see below). Anal. Calcd for $C_{55}H_{71}N_3I_2Yb_2$: C, 48.08; H, 5.21; N, 3.06. Found: C, 47.96; H, 5.07; N, 3.06. ^1H NMR (400.13 MHz, CD_2CN, 25 °C): δ 70.8 (2H, tpy), 30.1 (2H, tpy), 27.2 (2H, tpy), 22.4 (1H, tpy), 20.6 (2H, tpy), 17.1 (2H, tpy), 4.93 and 2.79 (30H, Cp*), 3.47 (30H, Cp*), −1.85 (30H, Cp*).

Preparation of [Cp*$_2$Yb^{III}(tpy)][PF$_6$] (6b). One equivalent of ferrocenium hexafluorophosphate (17.5 mg, 0.0531 mmol) was added to a solution of **1** (36.0 mg, 0.0531 mmol) in 5 mL of THF. The solution was stirred overnight until it gradually became a brown-orange suspension. The suspension was filtered, and the orange solid was collected on a medium-porosity frit and washed with toluene until the washings were colorless to give **6b** (32.0 mg, 0.0389 mmol) as an orange powder in 73% yield. ^1H NMR for **6b** (400.13 MHz, CD_2Cl_2, 25 °C): δ 71.3 (2H, tpy), 28.9 (2H, tpy), 26.0 (2H, tpy), 21.3 (1H, tpy), 20.6 (2H, tpy), 16.6 (2H, tpy), −2.19 (30H, Cp*).

Electrochemistry. Cyclic voltammetric studies were conducted in a Vacuum Atmospheres inert-atmosphere glovebox (nitrogen or helium) using a Perkin-Elmer Princeton Applied Research Corp. (PARC) model 263 potentiostat under computer control using M270 software. The electrochemical cell was a modified PARC microcell consisting of a ∼3 mm platinum disk working electrode, a Pt wire counter electrode, and a silver wire quasi-reference electrode. All experiments were conducted in purified THF using ∼0.1 M [(*n*-$C_4H_9)_4N$][$B(C_6F_5)_4$] as the supporting electrolyte. Measured potentials were calibrated using the ferrocene/ferrocenium couple. Data were analyzed using the IGOR Pro (Wavemetrics, Inc.) software package on a Macintosh platform.

Magnetic Susceptibility. Magnetic measurements over the temperature range of 2−350 K were made using a Quantum Design Superconducting Quantum Interference Device (SQUID) magnetometer. The microcrystalline samples were sealed in borosilicate NMR tubes along with a small amount of quartz wool, which held the sample near the tube center. Contributions to the magnetization from quartz wool and tube were measured independently and subtracted from the total measured signal. The magnetic susceptibility, defined as the sample magnetization *M* divided by the applied magnetic field *H*, was measured as a function of the temperature at applied fields of 0.1 T. Diamagnetic corrections were made using Pascal's constants.

X-ray Diffraction. Single-crystal X-ray diffraction experiments for **4** were performed on a Bruker P4diffractometer, with SMART 1K charge-coupled-device (CCD) detector and graphite-monochromated Mo Kα radiation (λ = 0.71073 Å). A crystal of **4** was coated with mineral oil and mounted on a glass fiber at −70 °C. A hemisphere of data was collected using a combination of φ and ω scans, with 30 s frame exposures and 0.3° frame widths. Data collection and initial indexing and cell refinement were performed using SMART[8] software. Frame integration and final cell parameter calculation were carried out using SAINT[9] software. The data were corrected for absorption using the SADABS[10] program.

Crystals of **5** and **6a** were mounted in a nylon cryoloop using mineral oil under an argon gas flow. The data were collected at −132 °C on a Bruker SMART APEX II CCD diffractometer, with a KRYO-FLEX liquid-nitrogen-vapor cooling device. The instrument was equipped with a graphite-monochromatized Mo Kα X-ray source (λ = 0.71073 Å), with MonoCap X-ray source optics. A hemisphere of data was collected using ω scans, with 5 s frame exposures and 0.3° frame widths. Data collection and initial indexing and cell refinement were handled using APEX II[11] software. Frame integration, including Lorentz polarization corrections, and final cell parameter calculations were carried out using SAINT+[12] software. The data were corrected for absorption using the SADABS[13] program.

The crystal and refinement parameters for **4**−**6a** are listed in Table 1. Decay of the reflection intensity was monitored via analysis of redundant frames. The structures were solved using direct methods and difference Fourier techniques. The hydrogen atoms were refined using a riding model, with their isotropic temperature factors set to 1.2 (aromatic, methyne, and methylene) or 1.5 (methyl) times the isotropic *U* of the attached carbon atom. The final refinement included anisotropic temperature factors on all non-hydrogen atoms. Structure solution, refinement, graphics,

(8) *SMART 4.210*; Bruker AXS, Inc.: Madison, WI, 1996.
(9) *SAINT 4.05*; Bruker AXS, Inc.: Madison, WI, 1996.
(10) *SADABS*; George Sheldrick, University of Göttingen: Göttingen, Germany, 1996.
(11) *APEX II 1.08*; Bruker AXS, Inc.: Madison, WI, 2004.
(12) *SAINT+ 7.06*; Bruker AXS, Inc.: Madison, WI, 2003.
(13) *SADABS 2.03*; George Sheldrick, University of Göttingen, Göttingen, Germany, 2001.

Table 1. Crystal Data and Structure Refinement Parameters for **4**, **5**, and **6a**

	4	**5**	**6a**
empirical formula	$C_{46.50}H_{58}Cl_3F_6N_3PYb$	$C_{37}H_{42}Cl_2IN_4Yb$	$C_{59}H_{79}I_2IN_3OYb_2$
formula weight	1083.32	913.59	1446.13
cryst syst	monoclinic	triclinic	orthorhombic
space group	$P2_1/c$	$P\bar{1}$	$Pna2_1$
a, Å	15.880(3)	8.5216(16)	15.9987(15)
b, Å	18.367(4)	10.743(2)	16.1466(15)
c, Å	18.158(3)	21.294(4)	21.478(2)
α, deg	90	80.713(3)	90
β, deg	112.589(4)	79.361(3)	90
γ, deg	90	75.470(3)	90
V, Å^3	4889.7(16)	1841.0(6)	5548.3(9)
Z	4	2	4
density (calcd), mg/m^3	1.472	1.648	1.731
abs coeff, mm^{-1}	2.166	3.554	4.504
F(000)	2192	898	2832
θ for data collection	1.64−28.21	1.96−25.35	1.58−28.12
limiting indices	$-20 \le h \le 20$ $-23 \le k \le 23$ $-23 \le l \le 17$	$-10 \le h \le 10$ $-10 \le k \le 12$ $-25 \le l \le 25$	$-20 \le h \le 20$ $-20 \le k \le 21$ $-28 \le l \le 17$
reflns collected	34713	12344	42164
independent reflns	10580 [R(int) = 0.0246]	6526 [R(int) = 0.0413]	10646 [R(int) = 0.0812]
completeness to $2\theta = 50.00°$	97.5%	96.9%	99.5%
refinement method	full matrix least squares on F^2	full matrix least squares on F^2	full matrix least squares on F^2
data/restraints/parameters	10580/3/546	6526/6/352	10646/1/579
goodness of fit on F^2	0.887	1.556	0.917
final R indices [$I > 2\sigma$I]	R1 = 0.0425, wR = 0.1117	R1 = 0.0823, wR = 0.2168	R1 = 0.0487, wR = 0.1058
R indices (all data)	R1 = 0.0631, wR2 = 0.1347	R1 = 0.0939, wR2 = 0.2218	R1 = 0.0838, wR2 = 0.1127
largest diff. peak and hole	1.651 and −0.840 e Å^{-3}	7.062 and −2.843 e Å^{-3}	2.605 and −2.217 e Å^{-3}

Table 2. IR C≡N Stretching Frequencies for tpyCN, tpyCN$^-$, **2**, **3**, and **5**

compound	IR ($\nu_{C\equiv N}$, cm^{-1})
tpyCN	2238 (Nujol)
K^+(tpyCN)$^-$	2149 (Nujol)
[Cp*$_2$Yb(η^3-tpyCN)] (**2**)	2172 ($C_6H_5CH_3$)
[Cp*$_2$Yb^{III} (η^3-tpyCN)]PF_6 (**3**)	2240 (Nujol)
[Cp*$_2$Yb^{III}(η^1-NCtpy)] (**5**)	2263 (Nujol)

and creation of publication materials were performed using SHELXTL.[14]

The refinement of **4** revealed a second CH_2Cl_2 molecule that was severely disordered across an inversion center. Further refinement of **5** revealed a minor twin as evidenced by the fact that there was significant electron density present in locations inconsistent with the molecular structure. This is supported by the presence of many reflections having $F_o^2 \gg F_c^2$.

Results and Discussion

Synthesis of tpyCN Complexes of Ytterbocene. The addition of 1 equiv of tpyCN to a solution of Cp*$_2$Yb^{II}(OEt$_2$) in toluene resulted in an immediate change from an olive green solution to a dark blue suspension. Concentration of the solution and filtration of the suspension lead to isolation of **2** as a dark blue powder in 91% yield. As shown in Scheme 1, we propose the structure of complex **2** to be similar to that of the fully characterized ytterbocene terpyridine complex, **1** (Figure 1),[4] with a Yb metal center coordinated to a tridentate tpyCN ligand. As presented in Table 2, the room-temperature IR spectrum for complex **2** contains a single C≡N stretching band at 2172 cm^{-1}. This frequency is intermediate between that of the free tpyCN ligand (2241 cm^{-1}) and the fully reduced ligand, K^+(tpyCN)$^-$ (2149 cm^{-1}), consistent with the formation of a partially reduced radical anion. Similar perturbations of C≡N stretching frequencies have been observed for charge-transfer complexes of 4′-cyanopyridine adsorbed onto copper surfaces and copper colloids (i.e., $\nu_{C\equiv N}$ = 2240 cm^{-1} for the neutral 4′-cyanopyridine complex and $\nu_{C\equiv N}$ = 2090 cm^{-1} for the reduced 4′-cyanopyridine ligand complex)[15] and for TCNQ materials for which partial charge transfer is known to occur.[16] While IR spectroscopy has been used to establish the presence of reduced diimine ligands in the Cp*$_2$Yb(L) system,[1] the C≡N stretching mode for **2** provides the additional insight into the π^* electron density distribution of the triimine ligand in **2** and potentially into the dynamics of the VT equilibrium (vide infra).

Complex **2** undergoes oxidation with ferrocinium hexafluorophosphate in THF to give the Yb^{III} complex **3** with a neutral tpyCN ligand ($\nu_{C\equiv N}$ = 2240 cm^{-1}; Table 2) as the major product (80% isolated yield) of the reaction (Scheme 1). Note that the C≡N stretching frequency in **3** is nearly identical with that of free tpyCN, consistent with the formulation of the ligand in this cationic complex as a neutral species. An unusual side product also forms during this oxidation reaction in which the nitrile group is cleaved from the terpyridine and a new C−C bond is formed between the terpyridine and a Cp* ring to give complex **4** (<5% yield as determined by GC/MS analysis of the hydrolysis products of the **3**/**4** reaction mixture; Scheme 1), which has been characterized by X-ray diffraction analysis (see below). The formation of **4** is probably a consequence of the reduced state of the tpyCN ligand in **2** at room temperature. Similar C−C-forming reactions have been observed by Birke and

(14) *SHELXTL 5.10*; Bruker AXS, Inc.: Madison, WI, 1997.
(15) (a) Rubim, J. C.; Sala, O. *J. Mol. Struct.* **1986**, *145*, 157−172. (b) Coyle, C. M.; Chumanov, G.; Jagodzinski, P. W. *J. Raman Spectrosc.* **1998**, *29*, 757−762.
(16) Chappell, J. S.; Bloch, A. N.; Bryden, W. A.; Maxfield, M.; Poehler, T. O.; Cowan, D. O. *J. Am. Chem. Soc.* **1981**, *103*, 2242−2246.

Scheme 1

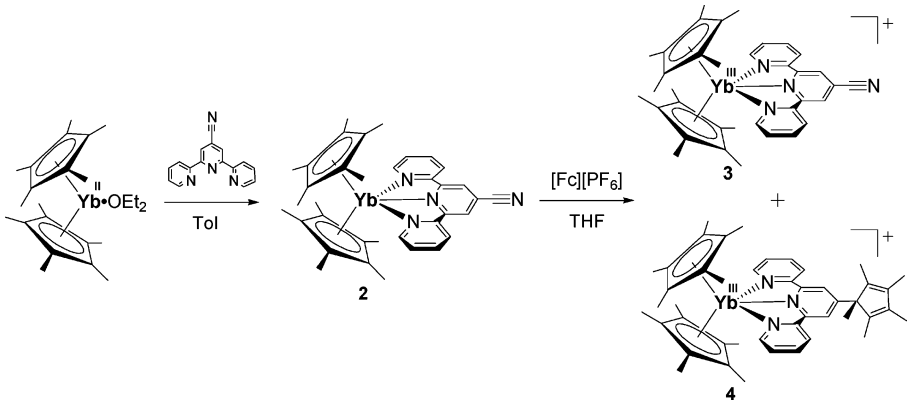

Scheme 2

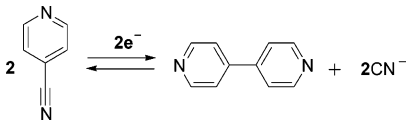

co-workers upon electrochemical reduction of 4′-cyanopyridine to provide bipyridine (Scheme 2).[17] To date, we have been unable to isolate X-ray quality crystals of **3**, but hydrolysis experiments and GC/MS data confirm that **3** is the major oxidation product. As expected for a paramagnetic Yb^{III} cation, the ^{1}H NMR spectrum of **3** reveals a strong paramagnetic shift of the tpyCN ligand protons, which resonate between 17.2 and 77.0 ppm in CD_2Cl_2. Furthermore, no methyl resonances associated with the $tpyC_5Me_5$ portion of **4** could be observed in the ^{1}H NMR spectrum of **3**.

Andersen and co-workers have also shown that stable ytterbocene bidentate N-heterocyclic neutral ligand complexes such as $[Cp^*_2Yb^{III}(phen)]I$ can be prepared by the reaction of $Cp^*_2Yb^{III}(THF)I$ with phen.[1] Hence, we reacted tpyCN with $Cp^*_2Yb^{III}(THF)I$ in CH_2Cl_2, but instead of forming the expected tridentate neutral ligand complex, the tpyCN ligand binds ytterbocene in an η^1-coordination mode through the nitrogen of the cyano group to form complex **5** (Scheme 3). Complex **5** has been characterized by X-ray diffraction analysis (see below) and its IR spectrum contains a strong $\nu_{C\equiv N}$ absorption at 2263 cm^{-1} (Table 2) consistent with monodentate coordination of the tpyCN ligand to ytterbium through the nitrogen of the cyano substituent (cf. $\nu_{C\equiv N}$ for N-bound 4′-cyanopyridine metal complexes[18]). To confirm that $Cp^*_2Yb^{III}(THF)I$ is a viable precursor to ytterbium tridentate tpy complexes, $Cp^*_2Yb^{III}(THF)I$ was treated with unsubstituted tpy to give the tridentate tpy complex **6a**. However, $Cp^*_2Yb^{III}(THF)I$ did not react with a full equivalent of tpy to give **6a** as an iodide salt but rather $[Cp^*_2Yb^{III}(tpy)][Cp^*_2Yb^{III}I_2]$ was isolated in 84% yield and characterized by X-ray diffraction analysis (see below) and ^{1}H NMR spectroscopy. Andersen and co-workers observed a similar result upon reaction of $Cp^*_2Yb^{III}(THF)Cl$ with bipyridine to form $[Cp^*_2Yb^{III}(bpy)][Cp^*_2Yb^{III}Cl_2]$, although they did not report this type of reaction for $Cp^*_2Yb^{III}(THF)I$.[1]

X-ray Diffraction. The X-ray structures of **4**, **5**, and **6a** are shown in Figures 2−4, and selected bond lengths and angles are listed in Table 3. The structures of **4** and **6a** clearly demonstrate that the $tpyC_5Me_5$ and tpy ligands are bound in a tridentate fashion within the ytterbocene wedge. Comparison of the structures of the neutral and cationic complexes of $Cp^*_2Yb(tpy)$ (**1** and **6a**) shows a lengthening of the central Yb−N distance from 2.41(1) to 2.432(9) Å between the neutral and oxidized forms (Table 3). The terminal Yb−N distances do not exhibit significant changes between the neutral and oxidized species, viz., 2.42(1) for the neutral form (**1**) and 2.397(9) and 2.445(10) Å for the cation (**6a**). The Yb−Cp* metrics are altered considerably upon going from **1** to **6a**. Average $Yb-Cp^*_{centroid}$ distances shorten from 2.44 to 2.38 Å from **1** to **6a**, while the Cp*−Yb−Cp* angle widens from 138.1 to 142.6°. These changes are consistent with those observed for $Cp^*_2Yb(bpy)$ and its cationic complex.[1] Bond distances and angles observed for **4** are consistent with those from its formulation as a Yb^{III} complex (Table 3).

The structure of **5** confirms that the tpyCN ligand is η^1-bound to the nitrile functionality. The Yb−N distance of 2.372(3) Å is the shortest to date reported for η^1-bound Yb−N≡C−R complexes. There are 15 reported structures in the Cambridge Structure Database[19] that have Yb−N distances that range from 2.419 to 2.621 Å. The C≡N bond distance for **5** [1.140(5) Å] does not appear to be altered by the strong Yb−N interaction because it falls well within the range of 1.103−1.148 Å for Yb−N≡C−R complexes. The Yb−I distance of 2.9218(5) Å falls within the short end of the range of 2.910−3.252 Å reported for nonbridging Yb−I complexes. The $Yb-Cp^*_{centroid}$ distance for complex **5** is 2.32 Å, and the Cp*−Yb−Cp* angle is 137.5°.

Electrochemistry. Recent cyclic voltammetry studies of ytterbocene imine complexes, including $Cp^*_2Yb(bpy)$, $Cp^*_2Yb(phen)$, and $Cp^*_2Yb(tpy)$, have established that the charge transfer ($4f^{14}-\pi^{*0} \Rightarrow 4f^{13}-\pi^{*1}$) in these complexes is consistent with a remarkable stabilization of the imine

(17) Shi, C.; Zhang, W.; Birke, R.; Lombardi, J. R. *J. Electroanal. Chem.* **1997**, *423*, 67−81.

(18) (a) Coerver, H. J.; Curran, C. *J. Am. Chem. Soc.* **1958**, *80*, 3522−3523. (b) Kubota, M.; Schulze, S. R. *Inorg. Chem.* **1964**, *3*, 853−856.

(19) ConQuest, version 1.6, new software for searching the Cambridge Structural Database and visualizing crystal structures. Bruno, I. J.; Cole, J. C.; Edgington, P. R.; Kessler, M.; Macrae, C. F.; McCabe, P.; Pearson, J.; Taylor, R. *Acta Crystallogr.* **2002**, *B58*, 389−397.

Scheme 3

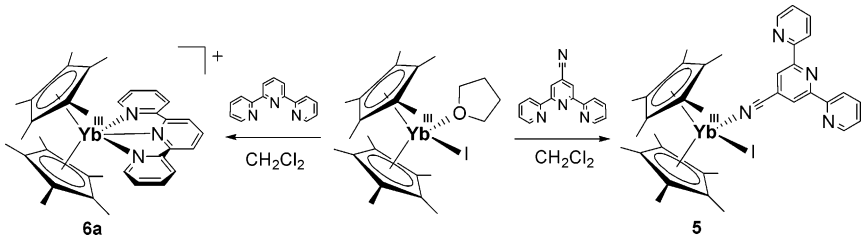

LUMO and concomitant destabilization of the ytterbium f orbitals.[3,4] Typical room-temperature cyclic voltammetric scans for 0.1 M $[(n\text{-}C_4H_9)_4N][B(C_6F_5)_4]$/THF solutions of **1** and **2** and for the uncomplexed (neutral) ligands and $Cp^*_2Yb^{II}(OEt_2)$ are shown in Figure 5, while potential data extracted from these scans are compiled in Table 4. The two reversible waves observed for complexes **1** and **2** have been assigned to a terpyridine ligand-based oxidation process and a metal-based reduction process that affirm the proposed metal-to-ligand electron transfer of **1** and **2**.[20] The voltammetric data for complex **2** are similar to the data obtained for **1** such that coordination stabilizes the tpyCN ligand LUMO by 890 mV and renders the ytterbium metal more difficult to reduce by 730 mV for complex **2**. Another significant aspect of these electrochemical data is the potential separation between the oxidation wave and reduction wave, established as $\Delta E_{1/2} = 900$ mV for **2** and $\Delta E_{1/2} = 840$ mV for **1**. This difference is a direct measure of the stability of the charge-transfer state relative to the fully oxidized ($4f^{13}-\pi^{*0}$) and fully reduced ($4f^{14}-\pi^{*1}$) forms of the complex (i.e., the larger the difference, the more stable the configuration).[21] Thus, the data imply that the $4f^{13}-\pi^{*1}$ configuration is more stable for the tpyCN complex, **2**, than for the tpy complex, **1**. Furthermore, both **1** and **2** are more stable in the $4f^{13}-\pi^{*1}$ configuration than the previously reported bpy ytterbocene complex, $Cp^*_2Yb(bpy)$ ($\Delta E_{1/2} = 790$ mV).[3] These observations suggest that an extension of the ligand π-electron system and the addition of an electron-withdrawing group stabilize the charge-transfer process through greater delocalization of the unpaired electron.

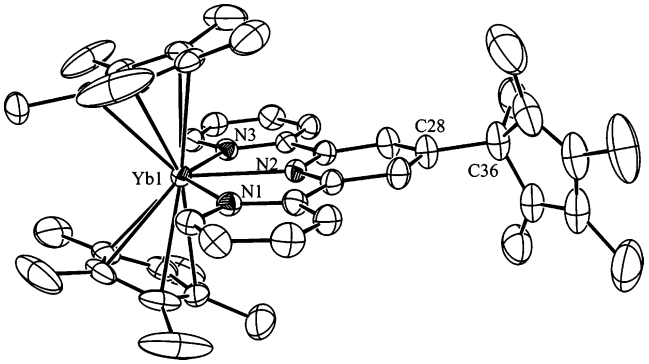

Figure 2. Thermal ellipsoid representation of **4** (35% probability ellipsoids). Two molecules of CH_2Cl_2, one unit of PF_6^-, and all hydrogen atoms have been omitted for clarity.

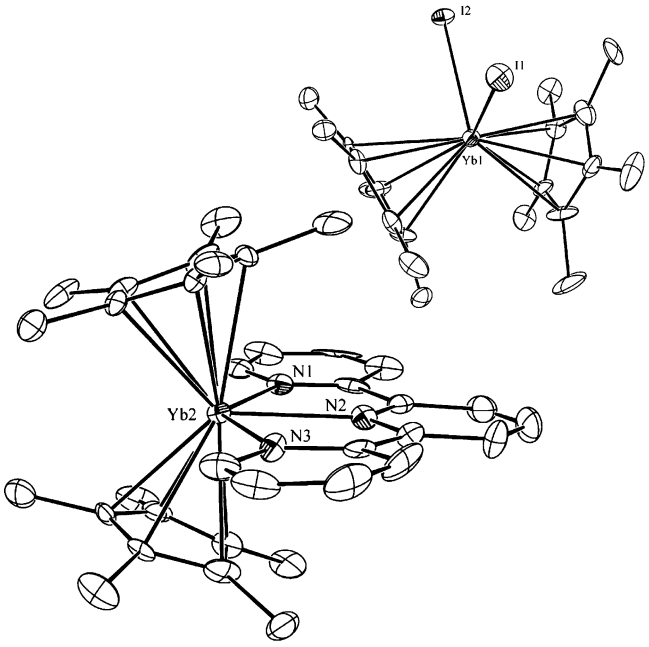

Figure 3. Thermal ellipsoid representations of the cation, $Cp^*_2Yb^{III}(tpy)^+$, and anion, $Cp^*_2Yb^{III}I_2^-$, of **6a** (35% probability ellipsoids). One molecule of THF and all hydrogen atoms have been omitted for clarity.

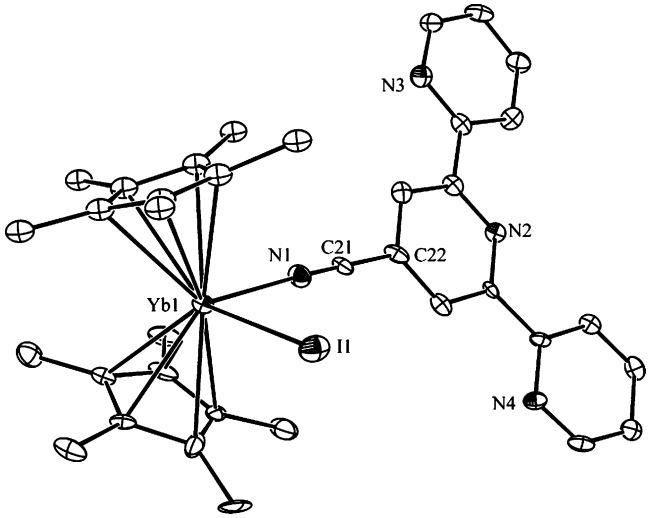

Figure 4. Thermal ellipsoid representation of **5** (35% probability ellipsoids). One molecule of CH_2Cl_2 and all hydrogen atoms have been omitted for clarity.

Magnetic Susceptibility. The magnetic susceptibilities (χ) for compounds **1**, **2**, and **6b** were measured as a function of

(20) The cyclic voltammogram for **2** contains a wave associated with a small impurity that is most likely associated with a side product of the oxidation of the reduced tpyCN ligand that is similar to the C−C-bond-forming reaction observed in the formation of **4** (Scheme 1).

(21) These voltammetric data do not provide information on the stability of the $4f^{13}-\pi^{*1}$ state relative to the diamagnetic ($4f^{14}-\pi^{*0}$) tautomer, although, in principle, the diamagnetic species should have a ligand-based reduction wave and a metal-based oxidation wave, and from this suite of redox potentials, the tautomeric equilibrium constant could be calculated. Low-temperature voltammetric experiments are being planned in an attempt to access these additional data.

Table 3. Selected Bond Lengths (Å) and Angles (deg) for **4**, **5**, and **6a**

	1[a]	**4**	**6a**		**5**
Yb−Cp*$_{centroid}$[b]	2.44	2.39	2.38	Yb−Cp*$_{centroid}$	2.32
Yb−N1	2.42(1)	2.435(4)	2.445(10)	Yb−N1	2.372(3)
Yb−N2	2.41(1)	2.432(4)	2.432(9)	Yb−I1	2.9218(5)
Yb−N3	2.42(1)	2.449(4)	2.397(9)	N1−C21	1.140(5)
C28−C36		1.530 (8)		N1−Yb−I1	87.12(7)
Cp*−Yb−Cp*	138.3	141.2	142.6	Cp*−Yb−Cp*	137.5
C37−C36−C45		110.4(8)		C21−N1−Yb	177.0(3)
Yb1−I1			2.9799(11)	N1−C21−C22	178.4(4)
Yb1−I2			2.9992(9)		
I1−Yb1−I2			90.01(3)		
Yb1−Cp*$_{centroid}$			2.353		
Cp*−Yb1−Cp*			135.7		

[a] See ref 4. [b] Average distance.

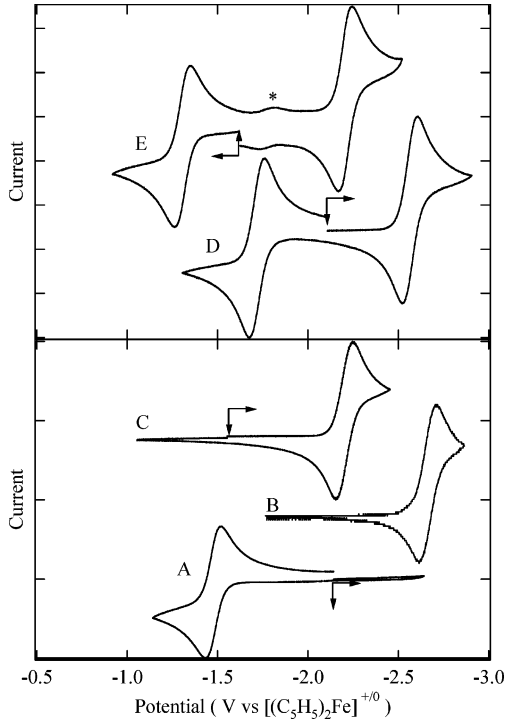

Figure 5. Cyclic voltammograms at a Pt disk working electrode in 0.1 M $[(n\text{-}C_4H_9)_4N][B(C_6F_5)_4]$/THF at room temperature: (A) $(C_5Me_5)_2Yb^{II}(THF)_n$; (B) terpyridine; (C) cyanoterpyridine; (D) $(C_5Me_5)_2Yb$(tpy), **1**; (E) $(C_5Me_5)_2Yb$(tpyCN), **2**. Concentrations of all analytes were ∼5 mM. Currents are in arbitrary units to facilitate comparisons. The vertical arrows indicate the rest potential for each system, and the horizontal arrows indicate the initial scan direction. The asterisk in part E denotes the wave from a small impurity.[20]

temperature (Figure 6). The temperature dependence in χT vs T for **6b** shows a gradual decrease from its value at 350 K of 2.26 emu K mol^{-1} (4.25 μ_B) to a value of 0.90 emu K mol^{-1} (2.68 μ_B) at 2 K due to depopulation of crystal field levels arising from the ground state $^2F_{7/2}$ term of the Yb^{III} ion.[22] This behavior is similar to that reported for [Cp*$_2$Yb^{III}(bpy)]I.[1]

Previous reports indicate that the room-temperature magnetic moment for Cp*$_2$Yb(bpy) (2.4 μ_B, 0.72 emu K mol^{-1}) is much less than that of Cp*$_2$Yb(phen) (4.0 μ_B, 2.0 emu K mol^{-1})[1] and that the moments of both complexes were less than expected for a simple Yb^{III} ion and an uncoupled organic radical (4.85 μ_B, 2.95 emu K mol^{-1}). The differences in the observed magnetic moment of these reported complexes from that predicted for uncoupled moments have been attributed to antiferromagnetic coupling of the Yb^{III} and organic radical unpaired electrons.[1] An alternative explanation invokes a thermal equilibrium between Yb^{II} and Yb^{III} complexes.[1,23] In the current study, we have chosen to compare the magnetic susceptibility data of **1** and **2** to Cp*$_2$Yb(bpy) and not to Cp*$_2$Yb(phen) because molecular orbital calculations have shown that the LUMOs of phen and bpy ligands differ significantly, with those of bpy being more like those of tpy.[24]

Table 4. Redox Potential Data for Cp*$_2$Yb Terpyridine Complexes and Constituents

species	$E_{1/2}$(ox) (V)[a]	$E_{1/2}$(red) (V)[a]	$\lvert\Delta E_{1/2}\rvert$(red/ox) (mV)
bpy[3]		−2.75	
tpy[4]		−2.66	
tpyCN		−2.20	
$(C_5Me_5)_2Yb^{II}(THF)_n$	−1.48		
$(C_5Me_5)_2Yb(bpy)$[3]	−1.67	−2.46	790
$(C_5Me_5)_2Yb(tpy)$ (**1**)[4]	−1.72	−2.56	840
$(C_5Me_5)_2Yb(tpyCN)$ (**2**)	−1.31	−2.21	900

[a] Potentials in volts versus $[(C_5H_5)_2Fe]^{+/0}$.

Below 350 K, the magnetic susceptibilities of both **1** and **2** depart significantly from a Curie law dependence expected for a collection of noninteracting Yb^{III}-free ions. As was observed in the case of Cp*$_2$Yb(bpy), the magnetic moments of **1** (3.77 μ_B, 1.77 emu K mol^{-1}) and **2** (4.44 μ_B, 2.46 emu K mol^{-1}) at 300 K are significantly less than expected for an uncoupled Yb^{III} ion and organic radical (4.85 μ_B, 2.95 emu K mol^{-1}). A plot of χT vs T exhibits an unusual sigmoidal-shaped response over the whole temperature range (Figure 6), dramatically dissimilar to the expected response for the sum of an isolated Yb^{III} ion and an organic radical. The unusual behavior of **1** and **2** is reflected in the plots of χ^{-1} vs T and χ vs T as broad maxima (Figure 6 and the Supporting Information). The overall temperature dependences of these susceptibilities are reminiscent of those found in complexes exhibiting VT[25] and some Yb-based interme-

(22) Boudreaux, E. A.; Mulay, L. N. *Theory and Applications of Molecular Paramagnetism*; John Wiley & Sons: New York, 1976.

(23) (a) Bochkarev, A. A.; Trifonov, F. G.; Cloke, G. N.; Dalby, C. I.; Matsunaga, P. T.; Andersen, R. A.; Schumann, H.; Loebel, J.; Hemling, H. *J. Organomet. Chem.* **1995**, *486*, 177−182. (b) Evans, W. J.; Drummond, D. K. *J. Am. Chem. Soc.* **1989**, *111*, 3329−3335.

(24) Ernst, S.; Vogler, C.; Klein, A.; Kaim, W.; Zališ, S. *Inorg. Chem.* **1996**, *35*, 1295−1300.

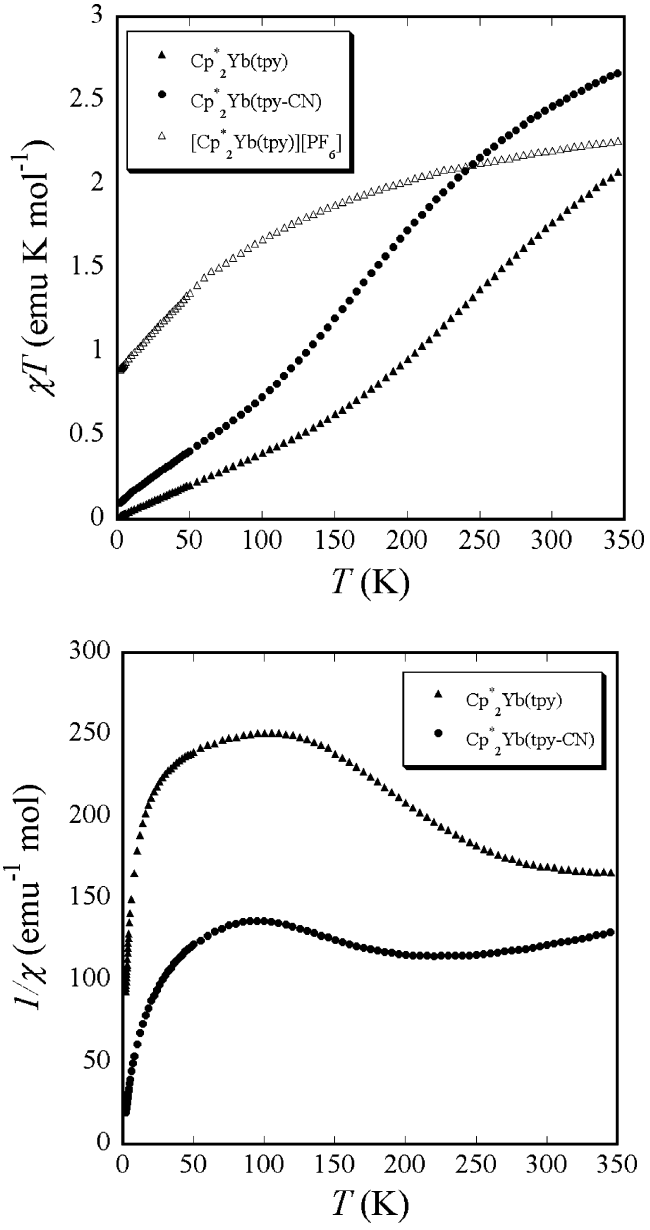

Figure 6. χT vs T of **1** (▲), **2** (●), and **6b** (△) (top) and χ^{-1} vs T plots of **1** (▲) and **2** (●) (bottom). The data were measured in an applied field of 0.1 T.

tallic mixed-valence compounds such as $YbAl_2$,[26] in which the valence configuration is nonintegral.

The preponderance of evidence across a variety of Ln/organic radical species indicates that magnetic coupling in these systems *does not* manifest itself at temperatures above ~60 K.[5,27] The unusual temperature dependence of the susceptibility of **2**, and indeed all of the Ln/imine complexes exhibiting this unusual behavior, is more consistent with that of a thermally induced VT rather than strong antiferromagnetic coupling. VT is a temperature-dependent equilibrium between two species having differing charge distributions between the metal center and a "noninnocent" (i.e., redox active) ligand and is frequently accompanied by a change in the spin state on the metal as well. This phenomenon has been extensively studied in Co/dioxolene complexes.[25] These cobalt complexes undergo a thermally induced metal-to-ligand charge-transfer process with a concomitant low-spin/high-spin transition on the metal, resulting in a dramatic change in their magnetic susceptibilities with temperature. The VT effect in the case of **1** and **2** does not include a metal-localized spin-state transition, but the temperature dependence of their magnetic moments results from a variable distribution of tautomers: the magnetic $4f^{13}-\pi^{*1}$ and the nonmagnetic $4f^{14}-\pi^{*0}$ species.

Using the high-temperature χT values for **1** and the magnetic data for **6b**, an approximation of the contributions from the paramagnetic $4f^{13}-\pi^{*1}$ and diamagnetic $4f^{14}-\pi^{*0}$ configurations to the observed moments in **1** can be made, with the additional assumptions that, within the paramagnetic fraction, the Yb^{III} ion contribution at the high-temperature limit (350 K) is purely that of the cation **6b** (4.25 μ_B, 2.26 emu K mol^{-1}) and the organic radical proportionally contributes 1.73 μ_B, 0.375 emu K mol^{-1}, to the paramagnetic fraction (i.e., the spin carriers are not coupled at this temperature). The calculation also assumes that the crystal field splittings of the $4f^{13}$ $^2F_{7/2}$ manifold in the neutral and cationic complexes are essentially the same. This approximation yields an 80% contribution of the $4f^{13}-\pi^{*1}$ configuration to the moment of **1** at 350 K (69% at 300 K). A similar approximation from the susceptibility data reported by Andersen and co-workers for the $Cp^*_2Yb(bpy)$ complex and its cation[1] yields a contribution of the $4f^{13}-\pi^{*1}$ configuration to the magnetic moment at 300 K of 28%. The impurity **4** observed in the oxidation of **2** prevents a quantitative analysis of the percentage of the $4f^{13}-\pi^{*1}$ configuration; however, the magnetic moment of **2** at 300 K and the electrochemical data indicate greater $4f^{13}-\pi^{*1}$ character in **2** than in **1** or $Cp^*_2Yb(bpy)$.

The temperature dependence of the χT vs T plots of **1** and **2** clearly indicates that the paramagnetic contribution to the magnetic moment is not scaled simply by a constant diamagnetic fraction over the whole temperature range. Rather, the sigmoidal nature of the curve indicates an additional component of temperature dependence to the magnetic susceptibility introduced by the VT of the complexes. As seen in Figure 6, the χT values for complexes **1** and **2** approach zero at low temperatures. This indicates that, in the VT description of the complexes, the equilibrium favors the diamagnetic $4f^{14}-\pi^{*0}$ configuration at low temperature.

Because of the VT effect present for **1** and **2**, it is not yet

(25) (a) Hendrickson, D. N.; Pierpont, C. G. *Topics in Current Chemistry*; Springer-Verlag: Berlin, 2004. (b) Schulz, D. A. *Magnetism: Molecules to Materials II: Molecule-Based Materials*; Wiley-VCH: Weinheim, Germany, 2002. (c) Pierpont, C. G. *Coord. Chem. Rev.* **2001**, *216*−*217*, 99. (d) Pierpont, C. G. *Coord. Chem. Rev.* **2001**, *219*−*221*, 415.

(26) For example, see: Lawrence, J. M.; Riseborough, P. S.; Parks, R. D. *Rep. Prog. Phys.* **1981**, *44*, 1−84 and references therein.

(27) (a) Kahn, M. L.; Sutter, J.-P.; Golhen, S.; Guionneau, P.; Ouahab, L.; Kahn, O.; Chasseau, D. *J. Am. Chem. Soc.* **2000**, *122*, 3413−3421. (b) Kahn, M. L.; Ballou, R.; Porcher, P.; Kahn, O.; Sutter, J.-P. *Chem. Eur. J.* **2002**, *8*, 525−531. (c) Sutter, J.-P.; Kahn, M. L.; Golhen, S.; Ouahab, L.; Kahn, O. *Chem. Eur. J.* **1998**, *4*, 571−576. (d) Kahn, M. L.; Ballou, R.; Porcher, P.; Kahn, O.; Sutter, J.-P. *Chemistry* **2002**, *8*, 525−531. (e) Benelli, C.; Gatteschi, D. *Chem. Rev.* **2002**, *102*, 2369−2387. (f) Benelli, C.; Caneschi, A.; Gatteschi, D.; Sessoli, R. *Inorg. Chem.* **1993**, *32*, 4797−801. (g) Caneschi, A.; Dei, A.; Gatteschi, D.; Poussereau, S.; Sorace, L. *Dalton Trans.* **2004**, *7*, 1048−1055.

possible to definitively determine whether these complexes exhibit any magnetic coupling between the unpaired electrons on the Yb^{III} metal ion and the terpyridine radical within the remaining paramagnetic fraction in the low-temperature regime ($<\sim$60 K). The divergence of the χ^{-1} vs T data at low temperatures hints at the possibility of residual paramagnetism arising from ferromagnetic coupling of the Yb^{III} and terpyridyl spin centers; however, the presence of a trace Yb^{III} impurity could also account for the divergence. The electronic lability of Ln/imine complexes has been noted previously[1,23] but not examined in the context of VT.

Theoretical Model. Additional support for this VT model comes from electronic structure calculations using hybrid density functional theory[29,30] employing the program Gausian03.[31]As a first model for these complexes, we studied the $Cp_2Yb(bpy)$ complex. We found that the optimum geometry corresponds to a diamagnetic, closed-shell, $4f^{14}$ configuration, with a predicted Yb−N(bpy) distance of 2.52 Å. Of those substituted Cp rings studied by Andersen, our Cp model is most similar to $[1,3\text{-}(Me_3C)_2C_5H_3]_2Yb(bpy)$,[1] which is also diamagnetic with an experimental Yb−N(bpy) distance of 2.503(4) Å. At the optimum geometry of the diamagnetic singlet, the $4f^{13}-\pi^{*1}$ triplet state lies some 2 eV higher in energy. In addition, we were not able to find a broken-symmetry solution corresponding to an antiferromagnetically coupled singlet diradical at this geometry. However, if the aforementioned triplet state is allowed to relax to its minimum (d[Yb−N(bpy)] = 2.35 Å), a singlet diradical solution containing a small moment on the Yb atom ($\rho_f \cong 0.25$) is found. This singlet diradical lies some 50 meV below the energy of the closed-shell, $4f^{14}$ diamagnetic state at this geometry and nearly 1 eV below the energy of the $4f^{13}-\pi^{*1}$ triplet state. We have not been able to find a local minimum for the singlet diradical because repeated attempts to optimize the geometry fall back to the diamagnetic ground-state basin. At the triplet geometry, the singlet diradical lies some 9 kcal/mol above the minimum energy for the diamagnetic ground state. We estimate that the spin−orbit correction might reduce this value to about 5 kcal/mol.

This work will be reported in more detail elsewhere,[32] but the basic picture to emerge from the calculations for $Cp_2Yb(bpy)$ is that of a significantly anharmonic potential curve connecting a diamagnetic closed-shell ground state with a mixed state comprised of 75% $4f^{14}$ character and 25% antiferromagnetically coupled $4f^{13}-\pi^{*1}$ singlet diradical character. We anticipate that changes in the ligand sets, either by modification of the electron-donating properties of the Cp ring or by manipulation of the energy of the acceptor levels of the imine ligand as was done in this work, may have an important effect on the energetic balance between the two states, resulting in profound differences in the resultant properties.

Summary and Conclusions

A new 4′-cyanoterpyridyl adduct of ytterbocene, **2**, has been prepared that exhibits physical properties (variable-temperature magnetic behavior, cyclic voltammetry, and IR spectroscopy) similar to those seen in other di- and triimine complexes of ytterbocene. These results clearly demonstrate that a paramagnetic charge-transfer state having the electronic configuration $4f^{13}-\pi^{*1}$ dominates at room temperature. However, the variable-temperature magnetic data for **2** and the structurally analogous **1** are most straightforwardly interpreted within the context of a VT equilibrium between this paramagnetic $4f^{13}-\pi^{*1}$ species and its diamagnetic tautomer having the electronic configuration $4f^{14}-\pi^{*0}$. A comparable VT is likely present in other di- and triimine base adducts of ytterbocene that show similar temperature-dependent magnetic behavior. In particular, this VT mechanism can account for both the small room-temperature magnetic moments observed for **1**, **2**, and $Cp^*_2Yb(bpy)$ and the sigmoidal shape of the χT vs T curves. The electron-withdrawing (−CN) substituent on the tpy ligand in **2** provides an added stability to the paramagnetic $4f^{13}-\pi^{*1}$ state of **2** relative to that of **1** and other base adducts of ytterbocene, as evidenced by the increased separation between the metal-based reduction and ligand-based oxidation waves in the voltammetry and the greater abundance of the $4f^{13}-\pi^{*1}$ state relative to the $4f^{13}-\pi^{*1}$ state in **2** at room temperature in comparison to those of the other ytterbocene adducts.

The physical data reported previously for these ytterbocene base adducts (e.g., voltammetry and electronic and resonance Raman spectroscopies)[3,4] did not explicitly take into account an equilibrium distribution of paramagnetic and diamagnetic species or the possibility that the diamagnetic state lies lowest in energy. However, these previous interpretations and descriptions are not compromised by this new finding of a VT because the data were all collected at or near room temperature where the paramagnetic state dominates and because the observable data (i.e., the resonance Raman or electronic transition intensity) is skewed in favor of this paramagnetic population (e.g., the oscillator strength in the

(28) For example, see: (a) Ito, T.; Hamaguchi, T.; Nagino, H.; Yamaguchi, T.; Kido, H.; Zavarine, I. S.; Richmond, T.; Washington, J.; Kubiak, C. P. *J. Am. Chem. Soc.* **1999**, *121*, 4625−4632. (b) Kubiak, C. P.; Londergan, C. H. *Chem. Eur. J.* **2003**, *9*, 5962−5969.

(29) The calculations utilize the hybrid B3LYP functional, the Stuttgart small-core relativistic effective core potential[30] and associated basis sets for Yb, and the 6-31g* basis set for the ligands.

(30) (a) Küchle, W.; Dolg, M.; Stoll, H.; Preuss, H. *J. Chem. Phys.* **1994**, *100*, 7535−7542. (b) Cao, X.; Dolg, M.; Stoll, H. *J. Chem. Phys.* **2003**, *118*, 487−496.

(31) Frisch, M. J.; Trucks, G. W.; Schlegel, H. B.; Scuseria, G. E.; Robb, M. A.; Cheeseman, J. R.; Montgomery, J. A., Jr.; Vreven, T.; Kudin, K. N.; Burant, J. C.; Millam, J. M.; Iyengar, S. S.; Tomasi, J.; Barone, V.; Mennucci, B.; Cossi, M.; Scalmani, G.; Rega, N.; Petersson, G. A.; Nakatsuji, H.; Hada, M.; Ehara, M.; Toyota, K.; Fukuda, R.; Hasegawa, J.; Ishida, M.; Nakajima, T.; Honda, Y.; Kitao, O.; Nakai, H.; Klene, M.; Li, X.; Knox, J. E.; Hratchian, H. P.; Cross, J. B.; Bakken, V.; Adamo, C.; Jaramillo, J.; Gomperts, R.; Stratmann, R. E.; Yazyev, O.; Austin, A. J.; Cammi, R.; Pomelli, C.; Ochterski, J. W.; Ayala, P. Y.; Morokuma, K.; Voth, G. A.; Salvador, P.; Dannenberg, J. J.; Zakrzewski, V. G.; Dapprich, S.; Daniels, A. D.; Strain, M. C.; Farkas, O.; Malick, D. K.; Rabuck, A. D.; Raghavachari, K.; Foresman, J. B.; Ortiz, J. V.; Cui, Q.; Baboul, A. G.; Clifford, S.; Cioslowski, J.; Stefanov, B. B.; Liu, G.; Liashenko, A.; Piskorz, P.; Komaromi, I.; Martin, R. L.; Fox, D. J.; Keith, T.; Al-Laham, M. A.; Peng, C. Y.; Nanayakkara, A.; Challacombe, M.; Gill, P. M. W.; Johnson, B.; Chen, W.; Wong, M. W.; Gonzalez, C.; Pople, J. A. *Gaussian 03*, revision C.02; Gaussian, Inc.: Wallingford, CT, 2004.

(32) Clark, A. E.; Martin, R. L., to be published.

electronic transitions of the radical anion ligand is greater and extends to lower energy than does that of the neutral ligand). Nonetheless, the challenge remains to devise additional experiments that reveal the presence of the diamagnetic tautomer at lower temperature. The existing IR vibrational data for the C≡N stretching mode in **2**, **3**, free tpyCN, and K(tpyCN) are intriguing but point out the potential difficulty in this task. In particular, the observation that $\nu_{C\equiv N}$ in **2** is intermediate between that in free tpyCN and that in K(tpyCN) could be an indication that there is a very rapid dynamic equilibrium between the paramagnetic and diamagnetic forms of **2** that leads to an averaging of this mode on the vibrational time scale. Such behavior has been reported for numerous mixed-valence systems.[28] Additional investigations are underway to further explore the effect of electron-withdrawing groups on ytterbocene N-heterocyclic charge-transfer complexes, additional physical manifestations of the VT effect, and the thermodynamics of the VT observed in this system. For example, preliminary variable-temperature ^{1}H NMR experiments on **1** and **2** allow observation of more of the tpy and tpyCN ligand localized resonances and afford peak sharpening at low temperatures with an increase in the diamagnetic fraction of **2**. Importantly, theoretical modeling of these complexes provides additional support for the VT model.

Finally, during the course of our investigation, we also discovered that tpyCN can form stable η^1 complexes with ytterbocene such that the ligand binds through the cyano nitrogen. This chemistry opens new paths to synthesize new homo-, hetero-, and multimetallic complexes, and new efforts to prepare these new higher order systems currently are in progress.

Acknowledgment. Support for this research was provided by the Los Alamos National Laboratory (LANL)'s Laboratory Directed Research and Development Office under Directed Research and Exploratory Research grants. The authors thank Drs. John L. Sarrao and Stuart A. Trugman (both of LANL) for helpful discussions. J.M.V. and E.J.S. thank the LANL G.T. Seaborg Institute for Transactinium Science for postdoctoral fellowships, C.J.K. thanks the U.S. Intelligence Community for a postdoctoral fellowship, and A.E.C. thanks LANL for a Director's postdoctoral fellowship. This research was performed at LANL under contract with the University of California (Contract W-7405-ENG-36).

Supporting Information Available: Full crystallographic details for **4**, **5**, and **6a** are available as CIF files, and plots of χ vs T for complexes **1** and **2** are also available. This material is available free of charge via the Internet at http://pubs.acs.org.

IC050148P